IEEE Photonics Journal
An IEEE Photonics Society Publication

Near-Infrared Soliton Mode-Locked Thulium Doped Fibre Laser Using WS_2-ZnO Composite Material as Saturable Absorber

(Invited Paper)

Volume 11, Number 5, October 2019

Harith Ahmad
Hadieh Monajemi
Muhammad Zharif Samion
Norazriena Yusoff
Mohd Faizal Ismail
Mohamad Yasin
Leonard Bayang

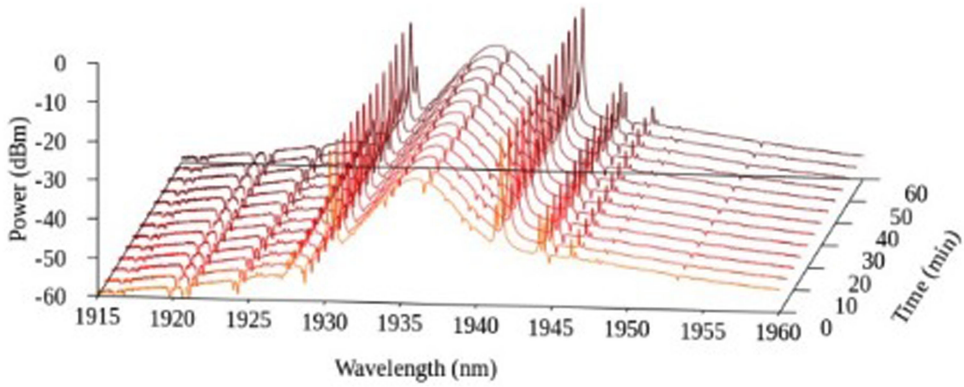

DOI: 10.1109/JPHOT.2019.2941286

Near-Infrared Soliton Mode-Locked Thulium Doped Fibre Laser Using WS_2-ZnO Composite Material as Saturable Absorber

(Invited Paper)

Harith Ahmad,[1,2,3] **Hadieh Monajemi**,[1] **Muhammad Zharif Samion**,[1] **Norazriena Yusoff**,[1] **Mohd Faizal Ismail**,[1] **Mohamad Yasin**,[3] **and Leonard Bayang**[1]

[1]Photonics Research Centre, University of Malaya, Kuala Lumpur 50603, Malaysia
[2]Physics Dept., Faculty of Science, University of Malaya, Kuala Lumpur 50603, Malaysia
[3]Department of Physics, Faculty of Science and Technology, Airlangga University, Surabaya 60115, Indonesia

DOI:10.1109/JPHOT.2019.2941286

Manuscript received July 31, 2019; revised September 3, 2019; accepted September 6, 2019. Date of publication September 23, 2019; date of current version October 7, 2019. This work was supported in part by the Ministry of Higher Education, Malaysia under Grants LRGS (2015)/ NGOD / UM / KPT and GA 010-2014 (ULUNG) and in part by the University of Malaya under Grants RU 013-2018 and HiCoE Funding Phase II. Corresponding authors: Harith Ahmad; Mohamad Yasin (e-mail: harith@um.edu.my; yasin@fst.unair.ac.id).

Abstract: The generation of a highly stable passive mode locking laser is realized in a thulium doped fibre laser using a WS_2-ZnO composite as a saturable absorber. Soliton mode locking pulses are generated with a central wavelength of 1936 nm and full-width half maximum (FWHM) of 3.06 nm. The first order Kelly's side band is located at around 5.65 nm from the central wavelength which gives the calculated pulse width value of 1.26 ps. This value corresponds well with the measured pulse width of 1.27 ps using the autocorrelator. The output power of the laser is around 0.44 mW with the peak power of 29.7 W and repetition rate of 9.96 MHz. This laser set-up is highly robust and realizes highly stable laser pulses in the mid-IR wavelength range for a multitude of applications.

Index Terms: Fiber Laser, Thulium, 2 micron.

1. Introduction

The strong association of vibrational transition characteristics of the mid-infrared spectral region with many important molecules makes 2 μm wavelength range laser sources highly beneficial for applications such as molecular spectroscopy, chemical sensing, materials processing, industry and free-space sensing [1]–[6]. Of particular interest would be the use of these lasers in industrial applications such as welding and cutting [7] as well as in minimal invasive surgery [8] due to their 'eye-safe' nature [9].

Fibre lasers operating at 2 μm are usually based on Thulium (Tm) [10], [11], Thulium-Holmium (Tm-Ho) [12], [13] and Holmium (Ho) [14], [15] doped fibres. Of these, Tm-doped fibre lasers (TDFL) are one of the most efficient, stable and highly developed laser sources which can generate highly stable sub picosecond mode-locking laser pulses [16]–[19]. There are many methods that

can generate ultra-short passive mode-locking laser pulses in an all-fibre laser system, among which is the use of saturable absorbers (SAs) such as carbon nanotubes (CNTs), [20], graphene [21], metal oxides (MOs) [22], black phosphorus (BP) [23] and topological insulators [24]–[26]. Of many new nanomaterials being explored and studied, transition metal dichalcogenides (TMDs) in particular has shown significant promise for application as an SA to generate mode-locked in 2 μm region [10], [27]–[30]. In this regard, researchers have focused their attention on the exploration of hybridizing TMD nanosheets with other materials including noble metals, oxides and so on. Modifying the intrinsic properties of TMDs by hybridizing them with other materials is one of the attractive approaches to overcome their constraints and thus to realize good performance for various kinds of applications. For instance, hybridizing TMDs with metal oxides forms a new binary composite material which possesses both the excellent optical properties of TMDs and strong mechanical qualities of metal oxide. Among various types of metal oxides, zinc oxide (ZnO) presents itself as one of the promising materials to be used as SA due to its high third order nonlinearity [31], [32] and ultrafast carrier dynamics [33]. The new composite material would have an added advantage whereby the bandgap can be altered by changing the number of layers. This is due to the layer-dependent bandgap of TMDs [34], a property absent in MOs. This gives a versatile and precise way to tailor the band structures of the new composite material, thereby maximizing its potential to better match optoelectronics devices. One of them is to adjust the bandgap as to accommodate saturable absorption over a wider wavelength range.

In this study, a mode-locked TDFL using a WS_2-ZnO composite based SA is proposed and demonstrated. The WS_2 is first prepared with liquid phase exfoliation (LPE) technique before being mixed with $Zn(OH)_2$ using a wet chemical method to form the WS_2-ZnO composite. The WS_2-ZnO SA device is fabricated by depositing the WS_2-ZnO composite on to a side polished fiber and the nonlinear optical performance of this SA is investigated by a balanced twin-detector measurement system. The compact all-fiber laser based on the WS_2-ZnO SA emits stable mode-locked pulses with central wavelength of 1936 nm, pulse duration of 1.27 ps and repetition rate of 9.96 MHz. This would be the first time, to the best of the author's knowledge, that a hybrid WS_2-ZnO has been proposed and demonstrated as a SA for mode-locked generation in 2 μm region.

2. Preparation and Characterization of WS_2-ZnO Composite

In order to prepare the WS_2-ZnO composite, exfoliated WS_2 sheets must be mixed with $Zn(OH)_2$ solution. The WS_2 sheets are prepared by the liquid phase exfoliation (LPE) technique to exfoliate the WS_2 bulk powder into the few-layer WS_2 sheets. First, 600 mg of WS_2 powder which is purchased from 2D Semiconductors, is added to a 60 mL of ethanol solution and ultrasonically diffused for 8 hours using a probe sonicator with 500 W power and an amplitude of 50%. The exfoliated WS_2 sheet which is in the form of a supernatant is then separated from the WS_2 flakes, i.e., the precipitate by centrifuging the suspension for 1 hour at 5000 rpm. The WS_2 sheets is then transferred and kept in a Scott bottle for the next process. The $Zn(OH)_2$ solution is then prepared by stirring a mixture of NaOH (1g), $Zn[CH_3COO]_2{\bullet}2H_2O$ (3g), and $NH_3{\bullet}H_2O$ (25 mL) at room temperature. Once all the powders are dissolved, the solution is slowly added to 65 mL of deionized water and simultaneously stirred until the $Zn(OH)_2$ solution is formed.

At the final stage, 20 mL of the $Zn(OH)_2$ solution is mixed and stirred rapidly with 20 mL of the exfoliated WS_2 solution for 2 hours at a temperature of 90°C. These two materials are bound together with a 5 mL solution of 0.1 M Cetyl trimethylammonium bromide (CTAB) which is added to the mixture and stirred continuously. The resultant product is then centrifuged for 30 minutes at 5000 rpm, washed with deionized water and dried at 60°C in the oven for more than 8 hours, forming the final WS_2-ZnO composite in powder form.

The characterization of the WS_2-ZnO composite material is carried out using Raman measurement, absorption spectrum and modulation depth analysis as given in Fig. 1. For the Raman measurement, a Renishaw inVia Raman microscope is used which is connected to a 514 nm line from an argon ion laser as the source of excitation. The result of the Raman measurements are given in Fig. 1(a). Two sharp peaks are observed at 353 cm^{-1} and 419 cm^{-1} which is an indication

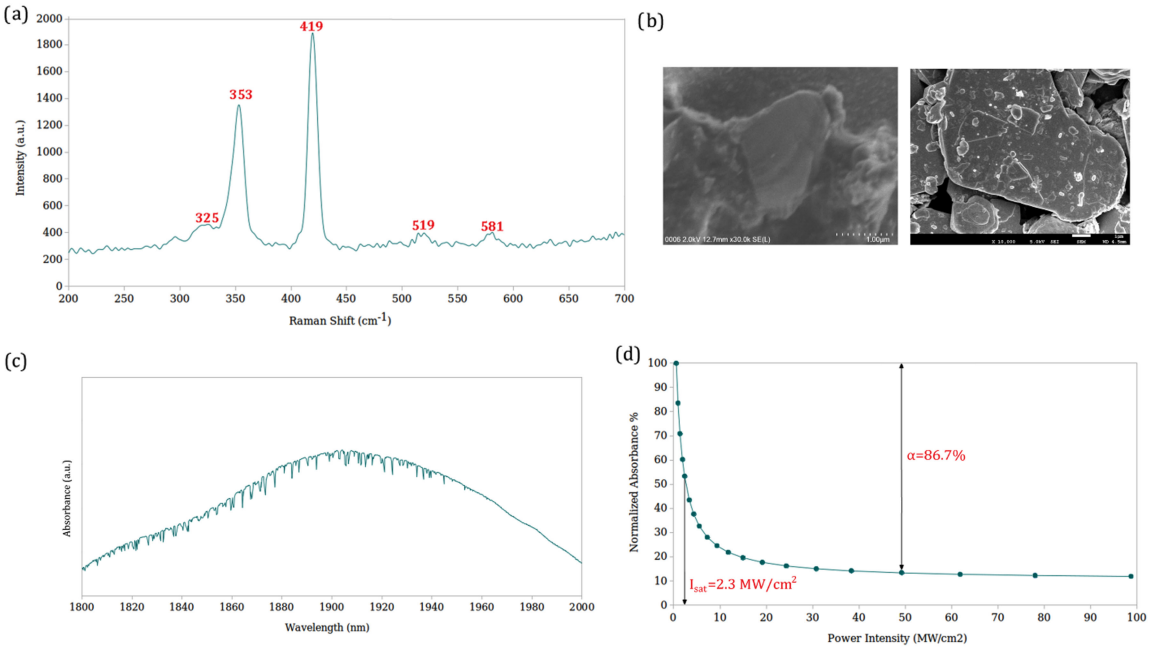

Fig. 1. (a) Raman spectrum of the WS_2–ZnO composite recorded at room temperature. (b) The FESEM images of WS_2 flakes at the left, and WS_2-ZnO composite on the right. (c) Absorption spectra of WS_2-ZnO composite at 2 μm range. (d) Modulation depth analysis of WS_2-ZnO composite.

of the in plane vibrational $E^1{}_{2g}$ mode as well as out of plane vibrational A_{1g} mode of the WS_2. This observation is in good agreement with the previous studies on the Raman spectroscopy of WS_2 [35], [36]. The other two peaks observed at 325 cm^{-1} and 581 cm^{-1} correspond to the $3E_{2H}$-E_{2L} multi photon scattering mode as well as E_1(LO) fundamental phonon mode of ZnO respectively [37], [38], while the weak peak at 519 cm^{-1} corresponds to the Si substrate [39]. The observed Raman peaks in the WS_2-ZnO composite indicates the proper formation of a composite between WS_2 and ZnO materials.

The results of surface morphological analysis of the WS_2 flakes and WS_2-ZnO composite which is carried out using an FEI Nova NanoSEM 400 field emission scanning electron microscope (FESEM) is given in Fig. 1(b). The left image represents the FESEM picture of WS_2 where the flaky shape of WS_2 with almost smooth surfaces is clearly defined. Upon adding the ZnO to WS_2, the ZnO particles are scattered on the smooth WS_2 flakes as shown in the right image of Fig. 1(b). This is an indication of a successful formation of the WS_2-ZnO composite.

The absorption measurement of the WS_2-ZnO saturable absorber is carried out by taking the amplified spontaneous emission (ASE) in the 2 μm region, from 1800 nm to 2000 nm, as it is shown in Fig. 1(c). The spectrum shows a smooth curve from 1900 nm to 1940 nm which peaks at around 1910 nm. This is in a good agreement with the previous study which has performed the near-infrared spectrum of ZnO [40].

UV-visible (UV-vis) absorption measurement is also carried out using a Varian Cary 50 UV–vis Spectrophotometer in the wavelength range of 300 to 800 nm. The UV–vis absorption spectra of the ZnO and WS_2-ZnO composite is shown in Fig. 2. From the absorption spectrum of ZnO, a peak at 377 nm can be observed and is attributed to the intrinsic band-gap absorption of ZnO caused by electron transitions from the valence to conduction bands ($O_{2p} \rightarrow Zn_{3d}$) [41]. Meanwhile, the absorption spectrum of the WS_2-ZnO composite shows peaks at around 411, 453, 520 and 628 nm. The appearance of peaks at 520 and 628 nm are attributed to the excitonic absorptions of the direct gap located at K point of the Brillouin zone [42], while the peaks at 411 and 453 nm are associated with the optical transitions from the valence band to conduction band [43]. It is noted

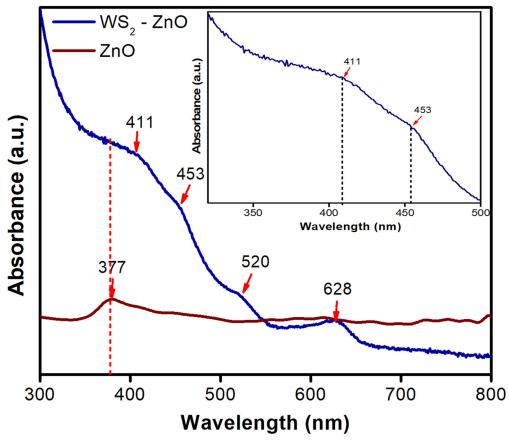

Fig. 2. UV-vis absorption spectra of ZnO and WS_2-ZnO composite. (Please note that the peak at 411 and 453 is not very distinct, but does indicate a very slight bump).

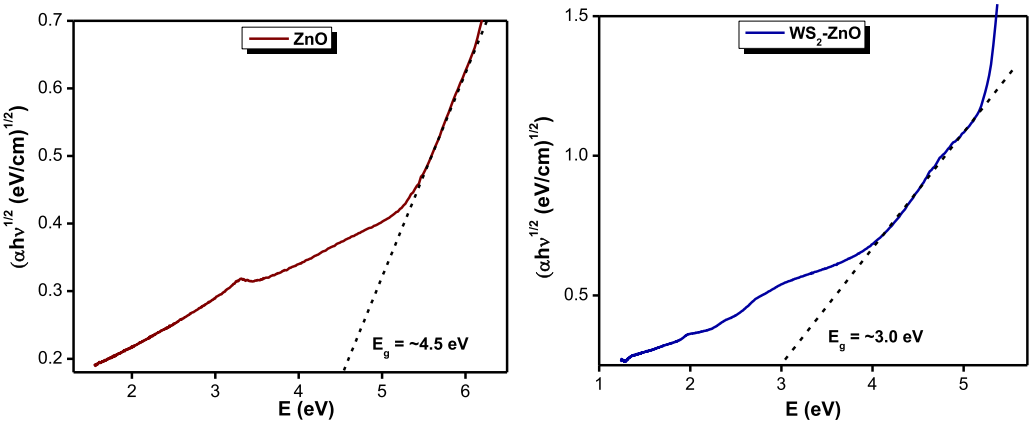

Fig. 3. Plot of $(\alpha h\nu)^{1/2}$ vs. $h\nu$ of (a) ZnO and (b) WS_2-ZnO composite.

that the absorption peak of ZnO could not be observed due to the strong WS_2 peak at 400 nm that has covered up the ZnO peak at 377 nm.

The band gap can be calculated from the equation [44]:

$$\alpha h\nu = A(h\nu - Eg)^n \tag{1}$$

where α is absorbance, h is Planck's constant, ν is the frequency, A is the proportional constant, n is equal to 2 and E_g is the band gap. Fig. 3 shows the plot of $(\alpha h\nu)^{1/2}$ *vs.* $h\nu$ of ZnO and the WS_2-ZnO composite. Extrapolation to $A = 0$ gives an absorption energy that corresponds to the band gap. The estimated band gap for ZnO and the WS_2-ZnO composite are calculated based on the Tauc's plot to be approximately 4.5 eV and 3.0 eV respectively. The difference in the bandgap values shows that the bandgap of the new composite material has indeed been altered as compared to its individual element.

Instead of the SA directly interacting with the propagating light, which might cause thermal damage at high operating power, the liquid form of WS_2-ZnO composite is deposited on a side polished fiber to interact with the evanescent field of the propagating light. At high optical intensity, the evanescent field interaction with WS_2-ZnO composite leads to a saturable absorption effect in the composite [45]–[47], which is then evaluated in the TDFL. In order to characterize the nonlinear optical properties of the device, the nonlinear absorbance of the WS_2-ZnO composite

on side polished fiber is measured using the balanced twin-detector method. An ELMO erbium femtosecond laser module is used as pulse source with a pulse width of $<$150 fs and output power of 5 dBm and repetition rate of 100 MHz in the wavelength range of 1564 nm. The calculated modulation depth is around 86% with the saturation intensity of 2.3 MW/cm^2 as shown in Fig. 1(d). This rather large modulation depth indicates the high pulse shaping ability of the SA which would then result in shorter pulse width. These characteristics are common for the SAs with rather large modulation depth which are studied previously [21], [48].

3. Experimental Setup

The WS_2-ZnO composite on a D-shaped fibre is used in a TDFL cavity with dual pumping scheme. The pump lasers are two Princeton Lightwave PSL-450 laser diodes (LDs) operating at 1560 nm, indicated as LD1 and LD2 in Fig. 2. A 1550 nm optical isolator is then connected to each LD to ensure that the light propagates in one direction without back reflection from the cavity to the LDs. The output of each isolator is spliced to the 1550 port of a 1550/2000 nm wavelength division multiplexer (WDM). The WDMs guide the 1550 nm light from the LDs to a 4 meter thulium-doped fiber (TDF) through their common ports. With the photons in 1550 nm range entering the doped fibre, the thulium dopants get excited to $^3F_4$ energy state and release photons in the range of 1700 nm to 2000 nm through stimulated emission process. The emitted photons are then guided by the 2000 nm port of both WDMs to the cavity. The 2000 nm port of the WDM1 is spliced to a 2000 nm isolator which prevents the light from reflecting back to the gain medium. The output of the isolator is then connected to a 90:10 coupler which extracts 10% of the light out for the measurement purposes. The 90% port of the coupler is then connected to a polarization controller (PC). The PC is used to adjust the optimal intra-cavity polarization to start the mode-locked operation. Finally, the cavity loop is closed by connecting the SA to the 2000 nm port of WDM2.

Initially, the mode locking pulse is detected and analyzed using a Keysight DSOX3102T oscilloscope (OSC) with the bandwidth of 1 GHz. To accurately measure the pulse width, an APE pulse check USB 150 autocorrelator is used. To convert the light into electrical signal, both the OSC and APE are connected to 818-BB-51F Newport 12.5 GHz InGaAs based photodetector. The optical spectrum is then measured and analyzed by a Yokogawa AQ6375 optical spectrum analyzer (OSA) with the spectral resolution of 0.02 nm. The mode locking pulse is then analyzed in frequency domain to check the fundamental pulse repetition rate and radio frequency pulse train by using Anritsu MS2683A radio frequency spectrum analyzer (RFSA) with frequency range between 9 kHz to 3 GHz.

The laser cavity operates at soliton mode locking regime which requires a net negative group velocity dispersion (GVD). The laser cavity contains two types of fibres, i.e., TDF and SMF-28, both of which induce the light to propagate in the negative dispersion regime. The TDF has the GVD parameter of -0.0213 ps^2/m which results in GVD of -0.085 ps^2 for the length of 4 meters in the cavity. The SMF-28 has the GVD parameter of -0.0696 ps^2/m which results in the GVD of -1.2 ps^2 for the length of 17.2 meters in the cavity. Hence, the net dispersion for the whole cavity of 21.2 meters is -1.3 ps^2.

4. Results

To achieve mode locking operation, the pump power is increased to 158 mW while the polarization state of the laser cavity is adjusted by the PC. This results in mode locking pulses with the repetition rate of 70 MHz which is at the sixth harmonic. In order to obtain the fundamental frequency, the pump power is reduced to 106 mW. For the cavity length of 23 meters and refractive index of 1.45 for silica fibre, the calculated value of fundamental frequency is around 9.8 MHz which is in good agreement with the observed value of 9.96 MHz by the oscilloscope trace as shown in Fig. 3(a). The pulse interval of 0.1 μs is also in a good agreement with the cavity round trip time.

The mode locking laser operates at soliton regime which can be clearly seen by the appearance of Kelly's sidebands in the optical spectrum in Fig. 5(b). The optical spectrum shows the central

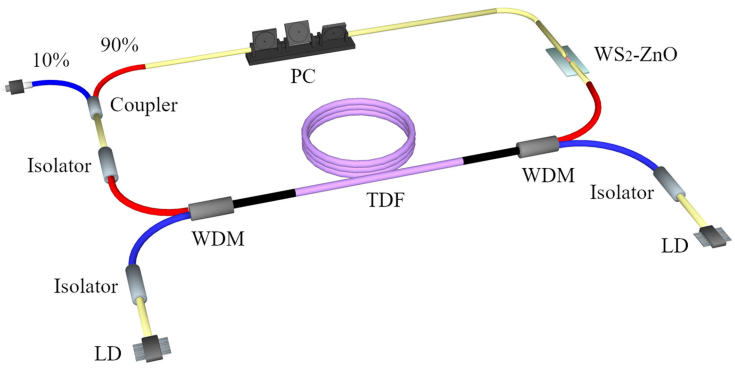

Fig. 4. Schematic view of the TDFL cavity setup.

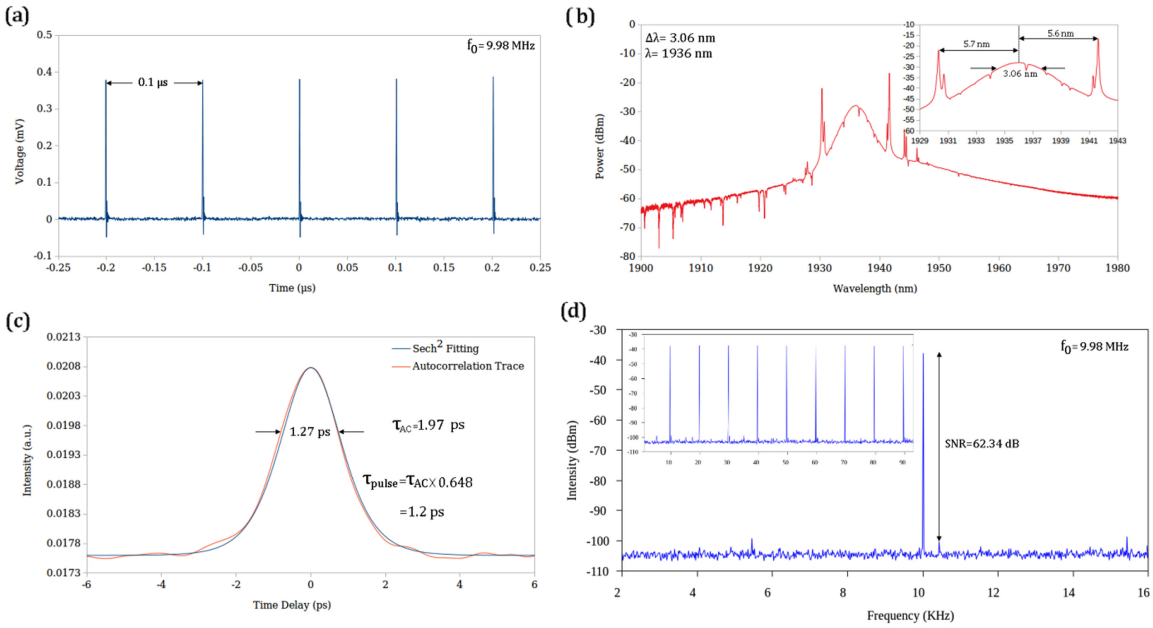

Fig. 5. (a) The oscilloscope pulse train with the fundamental frequency of 9.96 MHz. (b) The optical spectrum of the soliton mode locking pulse measured at the fundamental frequency of 9.96 MHz and the pump power of 106 mW. (c) The autocorrelation trace of the mode locking pulse. (d) The RF spectrum at fundamental frequency with the higher harmonics of the repetition rate illustrated in the inset.

wavelength of 1936 nm with the full width half maximum (FWHM) value of 3.06 nm. This value can approximately predict the temporal pulse duration by using the time bandwidth product (TBP) equation [49]. Assuming the minimum value of 0.315 for the sech^2 curve fitting, the TBP equation gives the minimum value of 1.2 ps. Another way to estimate the temporal pulse duration from the optical spectrum is by the position of the mth order of Kelly's sidebands with respect to the central wavelength in the optical spectrum using the following equation [50]:

$$\Delta\lambda = \frac{2ln\left(1+\sqrt{2}\lambda^2\right)}{2\pi c\tau}\sqrt{\frac{4m\pi}{|L\beta|}\left[\frac{\tau}{2ln\left(1+\sqrt{2}\right)}\right]^2 - 1} \tag{2}$$

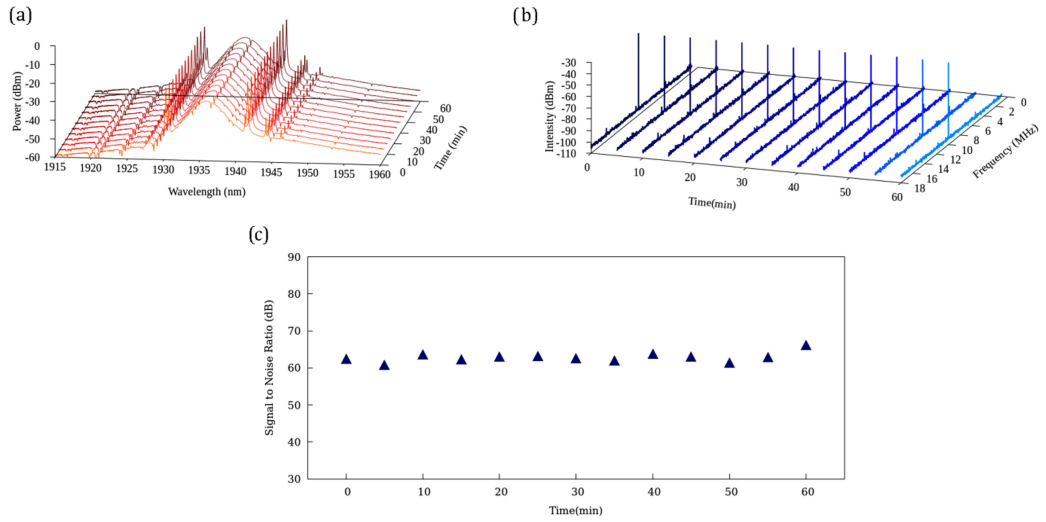

Fig. 6. The laser stability test, taken from the output of the pulsed laser over an hour with 5 minutes time intervals for (a) the optical spectra and (b) the RF spectra, and (c) the calculated SNR values from the RF spectra taken for an hour with 5 minutes time interval.

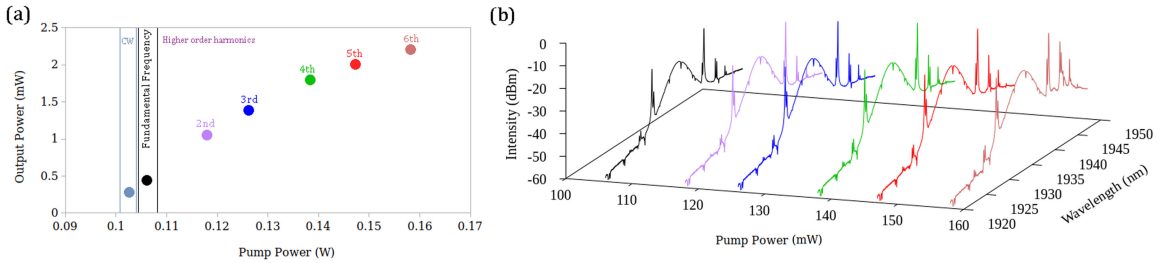

Fig. 7. (a) The output power versus the pump power. (b) Optical spectrum evolution with increasing the pump power.

where λ is the central wavelength, m is the order of the Kelly's sideband which is located at the distance of $\Delta\lambda$ with respect to the central wavelength, c is the speed of light, L is the length of the cavity and β is the cavity's GVD parameter. For the $\Delta\lambda$ value of around 5.65 nm for the 1st order Kelly's sideband as shown in the inset of Fig. 5(b) and central wavelength of 1936 nm, the calculated temporal pulse duration, τ, is around 1.26 ps. The actual pulse width is also measured using the APE PulseCheck autocorrelator, with the temporal pulse shape following the sech^2 fitting, as shown in Fig. 5(c). The measured value is 1.27 which is in good agreement with both calculated values of 1.2 ps using TBP and 1.26 ps using the position of Kelly's sideband.

The RF spectrum is presented in Fig. 5(d) which shows the high stability of the laser oscillator at the pump power of 106 mW. The signal to noise ratio (SNR) is around 62.3 dB which is higher than the required value for the laser to be applicable in telecommunication systems [51]. Fig. 4 illustrates the stability test of the pulsed laser which is carried out for two hours within 5 minutes time interval by taking the optical spectrum for one hour as shown in Fig. 6(a), and RF spectrum for the second hour as shown in Fig. 6(b). Both spectra show no change within the hour which confirms that the pulsed laser is highly stable. This is further validated by the similar SNR values from the RF spectra as shown in Fig. 6(c).

All the measurements are taken at the pump power of 106 mW. By decreasing the pump power below this value, the mode locking laser pulses disappears and the laser operates at continuous wave (CW) as shown in Fig. 7(a). However, increasing the pump power to 158 mW self-starts the mode locking laser pulses without having to re-adjust the PC. Once the pump power is increased,

TABLE 1
Comparison of 2 μm Mode-Locked Fiber Lasers Performances

SA	Method of incorporation	Gain fiber	Center wavelength (nm)	Rep. rate (MHz)	Pulse width (ps)	Pulse energy (pJ)	SNR	Ref
BP	Thin film	Tm	1910	36.8	0.74	40.7	70	[55]
CNT	Thin film	Tm	1927	25.7	0.15	190	73	[11]
WS_2	Deposited on tapered fiber	Tm-Ho	1916	15.49	1.27	18.2	67	[57]
WS_2	Deposited on side polished fiber	Tm-Ho	1941	34.8	1.3	17.2	72	[53]
WS_2	Thin film	Tm-Ho	1883	23.8	1070	440	NR	[52]
ZnO	Thin film	Tm	1945	11.36	1.395	56.33	50.5	[54]
WS_2-ZnO	Deposited on side polished fiber	Tm	1936	9.96	1.27	30	62	This work

Note: Rep: Repetition and NR: Not reported.

the output power is also increased and the laser operates at higher order harmonics. It however, does not affect the optical spectrum and as it can be seen in Fig. 7(b), the optical spectra and consequently the pulse width are not affected by increasing the pump power.

The output performances of this laser are compared with that of 2 μm mode-locked fiber lasers incorporating BP, CNT WS_2 and ZnO based SAs and summarized in Table 1. From this comparison, it can be seen that despite of having long cavity length, the output's pulse width of this work is shorter than those from the systems utilizing WS_2-based SAs [52], [53] and the ZnO-based SA [54]. From the table, narrower pulse widths can be obtained through the use of BP and CNT as shown by Sotor *et al.* [55] and Wang *et al.* [11] respectively, and therefore the pulse width and repetition rate of the cavity in this work can be improved by optimizing the laser cavity's length. This has been experimentally proven by Yang *et al.* [56], where shorter pulse widths are obtained for shorter cavity lengths. Additionally, although the pulse energy obtained in this work is not as high as that obtained by Yang *et al.* [52], its performance is comparable to the BP- and ZnO-based SAs and higher than that reported by systems utilizing WS_2-based SAs on tapered and side polished fibers. It is important to note that this work is among the few that reports a mode-locked TDFL with a central wavelength near 2000 nm. Furthermore, the SNR is comparable to other reported works at shorter wavelengths, indicating stable mode-locking operation. The proposed SA shows competitive performance with other SAs, and it can be concluded that the WS_2-ZnO composite is a good candidate for inducing mode-locking in fiber lasers at the 2 μm region.

5. Conclusions

In this study, a highly stable mode locking laser with the pulse width of 1.27 ps and repetition rate of 9.98 MHz is demonstrated. This laser set-up shows reliable self-starting mode locked pulses which is partially due to the large modulation depth of the WS_2-ZnO SA of 86.7%. The large SNR value of 62.3 dB and central wavelength of 1936 nm makes this laser highly stable and applicable in the areas of research which require ultrafast pulses in the eye safe region.

References

[1] Y. Wang, S. Y. Set, and S. Yamashita, "Active mode-locking via pump modulation in a Tm-doped fiber laser," *APL Photon.*, vol. 1, no. 7, 2016, Art. no. 71303.
[2] N. M. Fried and K. E. Murray, "High-power thulium fiber laser ablation of urinary tissues at 1.94 μm," *J. Endourol.*, vol. 19, no. 1, pp. 25–31, 2005.
[3] J. Wang *et al.*, "High-energy and efficient Raman soliton generation tunable from 1.98 to 2.29 μm in an all-silica-fiber thulium laser system," *Opt. Lett.*, vol. 42, no. 18, pp. 3518–3521, 2017.
[4] B. Hitz, "Two-micron fiber laser has potential for military and civilian applications," *Photon. Spectra*, vol. 41, no. 3, pp. 241–243, 2007.
[5] K. Minoshima, A. M. Kowalevicz, E. P. Ippen, and J. G. Fujimoto, "Fabrication of coupled mode photonic devices in glass by nonlinear femtosecond laser materials processing," *Opt. Exp.*, vol. 10, no. 15, pp. 645–652, 2002.
[6] S. W. Henderson *et al.*, "Coherent laser radar at 2 μm using solid-state lasers," *IEEE Trans. Geosci. Remote Sens.*, vol. 31, no. 1, pp. 4–15, Jan. 1993.
[7] I. Mingareev, F. Weirauch, A. Olowinsky, L. Shah, P. Kadwani, and M. Richardson, "Welding of polymers using a 2 μm thulium fiber laser," *Opt. Laser Technol.*, vol. 44, no. 7, pp. 2095–2099, 2012.
[8] S. Kharitonov and C.-S. Bres, "Isolator-free unidirectional thulium-doped fiber laser," *Light Sci. Appl.*, vol. 4, no. 10, 2015, Art. no. e340.
[9] J. Hecht, "Retina-safe wavelengths benefit open-air applications," *Laser Focus World*, vol. 44, no. 3, pp. 89–92, 2008.
[10] J. Wang *et al.*, "Ultrafast thulium-doped fiber laser mode locked by monolayer WSe 2," *IEEE J. Sel. Top. Quantum Electron.*, vol. 24, no. 3, pp. 1–6, May/Jun. 2018.
[11] J. Wang *et al.*, "152 fs nanotube-mode-locked thulium-doped all-fiber laser," *Sci. Rep.*, vol. 6, no. July, pp. 4–10, 2016.
[12] R. Gumenyuk, I. Vartiainen, H. Tuovinen, and O. G. Okhotnikov, "Dissipative dispersion-managed soliton 2 μm thulium/holmium fiber laser," *Opt. Lett.*, vol. 36, no. 5, pp. 609–611, 2011.
[13] R. Kadel and B. R. Washburn, "All-fiber passively mode-locked thulium/holmium laser with two center wavelengths," *Appl. Opt.*, vol. 51, no. 27, pp. 6465–6470, 2012.
[14] A. Chamorovskiy *et al.*, "Femtosecond mode-locked holmium fiber laser pumped by semiconductor disk laser," *Opt. Lett.*, vol. 37, no. 9, pp. 1448–1450, 2012.
[15] A. Y. Chamorovskiy, A. V Marakulin, A. S. Kurkov, and O. G. Okhotnikov, "Tunable Ho-doped soliton fiber laser mode-locked by carbon nanotube saturable absorber," *Laser Phys. Lett.*, vol. 9, pp. 602–606, 2012.
[16] Z. Yan *et al.*, "Widely tunable Tm-doped mode-locked all-fiber laser," *Sci. Rep.*, vol. 6, 2016, Art. no. 27245.
[17] Q. Fang, K. Kieu, and N. Peyghambarian, "An all-fiber 2-μm wavelength-tunable mode-locked laser," *IEEE Photon. Technol. Lett.*, vol. 22, no. 22, pp. 1656–1658, Nov. 2010.
[18] R. C. Sharp, D. E. Spock, N. Pan, and J. Elliot, "190-fs passively mode-locked thulium fiber laser with a low threshold," *Opt. Lett.*, vol. 21, no. 12, pp. 881–883, 1996.
[19] Y. Baravets, F. Todorov, and P. Honzatko, "High-power thulium-doped fiber laser in an all-fiber configuration," *Proc. SPIE*, vol. 10142, 2016, Art. no. 101420G.
[20] M. A. Solodyankin *et al.*, "Mode-locked 1.93 μm thulium fiber laser with a carbon nanotube absorber," *Opt. Lett.*, vol. 33, no. 12, pp. 1336–1338, 2008.
[21] G. Sobon, "Mode-locking of fiber lasers using novel two-dimensional nanomaterials: Graphene and topological insulators," *Photon. Res.*, vol. 3, no. 2, pp. A56–A63, 2015.
[22] H. Ahmad, M. Z. Samion, and N. Yusoff, "Soliton mode-locked thulium-doped fiber laser with cobalt oxide saturable absorber," *Opt. Fiber Technol.*, vol. 45, pp. 122–127, 2018.
[23] J. Li *et al.*, "Black phosphorus: A two-dimension saturable absorption material for mid-infrared Q-switched and mode-locked fiber lasers," *Sci. Rep.*, vol. 6, 2016, Art. no. 30361.
[24] H. Liu *et al.*, "Femtosecond pulse generation from a topological insulator mode-locked fiber laser," *Opt. Exp.*, vol. 22, no. 6, pp. 6868–6873, 2014.
[25] J. Sotor, G. Sobon, and K. M. Abramski, "Sub-130 fs mode-locked Er-doped fiber laser based on topological insulator," *Opt. Exp.*, vol. 22, no. 11, pp. 13244–13249, 2014.
[26] J. Sotor, G. Sobon, W. Macherzynski, and K. M. Abramski, "Harmonically mode-locked Er-doped fiber laser based on a Sb_2Te_3 topological insulator saturable absorber," *Laser Phys. Lett.*, vol. 11, no. 5, 2014, Art. no. 55102.
[27] J. Wang *et al.*, "Mode-locked thulium-doped fiber laser with chemical vapor deposited molybdenum ditelluride," *Opt. Lett.*, vol. 43, no. 9, pp. 1998–2001, 2018.
[28] J. Lee, J. Koo, J. Lee, Y. M. Jhon, and J. H. Lee, "All-fiberized, femtosecond laser at 1912 nm using a bulk-like $MoSe_2$ saturable absorber," *Opt. Mater. Exp.*, vol. 7, no. 8, pp. 2968–2979, 2017.
[29] Z. Tian *et al.*, "Mode-locked thulium fiber laser with MoS_2," *Laser Phys. Lett.*, vol. 12, no. 6, 2015, Art. no. 65104.
[30] J. Wang *et al.*, "Magnetron-sputtering deposited WTe_2 for an ultrafast thulium-doped fiber laser," *Opt. Lett.*, vol. 42, no. 23, pp. 5010–5013, 2017.
[31] C. Soci *et al.*, "ZnO nanowire UV photodetectors with high internal gain," *Nano Lett.*, vol. 7, no. 4, pp. 1003–1009, 2007.
[32] G. I. Petrov, V. Shcheslavskiy, V. V Yakovlev, I. Ozerov, E. Chelnokov, and W. Marine, "Efficient third-harmonic generation in a thin nanocrystalline film of ZnO," *Appl. Phys. Lett.*, vol. 83, no. 19, pp. 3993–3995, 2003.
[33] J. C. Johnson *et al.*, "Ultrafast carrier dynamics in single ZnO nanowire and nanoribbon lasers," *Nano Lett.*, vol. 4, no. 2, pp. 197–204, 2004.
[34] H.-C. Kim *et al.*, "Engineering optical and electronic properties of WS_2 by varying the number of layers," *ACS Nano*, vol. 9, no. 7, pp. 6854–6860, 2015.
[35] H. Zeng *et al.*, "Optical signature of symmetry variations and spin-valley coupling in atomically thin tungsten dichalcogenides," *Sci. Rep.*, vol. 3, 2013, Art. no. 1608.
[36] J. M. Woods *et al.*, "One-step synthesis of MoS_2/WS_2 layered heterostructures and catalytic activity of defective transition metal dichalcogenide films," *ACS Nano*, vol. 10, no. 2, pp. 2004–2009, 2016.

[37] S. Ameen, M. S. Akhtar, H.-K. Seo, Y. S. Kim, and H. S. Shin, "Influence of Sn doping on ZnO nanostructures from nanoparticles to spindle shape and their photoelectrochemical properties for dye sensitized solar cells," *Chem. Eng. J.*, vol. 187, pp. 351–356, 2012.
[38] M. Silambarasan, S. Saravanan, and T. Soga, "Mn-doped ZnO nanoparticles prepared by solution combustion method," *e-J. Surf. Sci. Nanotechnol.*, vol. 12, pp. 283–288, 2014.
[39] C. X. Xu, X. W. Sun, B. J. Chen, P. Shum, S. Li, and X. Hu, "Nanostructural zinc oxide and its electrical and optical properties," *J. Appl. Phys.*, vol. 95, no. 2, pp. 661–666, 2004.
[40] J. Brijitta, D. Ramachandran, K. Chennakesavulu, S. Bera, A. M. Rabel, S. S. Prasath, and K. R. Mary, "Mesoporous ZnO–SiO_2 core–shell rods for UV absorbing and non-wetting applications," *Mater. Res. Exp.*, vol. 3, no. 2, 2016, Art. no. 25001.
[41] A. K. Zak, R. Razali, W. H. A. Majid, and M. Darroudi, "Synthesis and characterization of a narrow size distribution of zinc oxide nanoparticles," *Int. J. Nanomedicine*, vol. 6, pp. 1399–1403, 2011.
[42] S. Sharma, S. Bhagat, J. Singh, R. C. Singh, and S. Sharma, "Excitation-dependent photoluminescence from WS_2 nanostructures synthesized via top-down approach," *J. Mater. Sci.*, vol. 52, no. 19, pp. 11326–11336, 2017.
[43] A. Bayat and E. Saievar-Iranizad, "Synthesis of blue photoluminescent WS_2 quantum dots via ultrasonic cavitation," *J. Lumin.*, vol. 185, pp. 236–240, 2017.
[44] S. Pati, P. Banerji, and S. B. Majumder, "Properties of indium doped nanocrystalline ZnO thin films and their enhanced gas sensing performance," *RSC Adv.*, vol. 5, no. 75, pp. 61230–61238, 2015.
[45] L. Miao *et al.*, "Erbium-doped fiber laser mode-locked by halide perovskite via evanescent field interaction," *IEEE Photon. Technol. Lett.*, vol. 30, no. 6, pp. 577–580, Mar. 2018.
[46] J. D. Zapata, D. Steinberg, L. A. M. Saito, R. E. P. De Oliveira, A. M. Cárdenas, and E. A. T. De Souza, "Efficient graphene saturable absorbers on D-shaped optical fiber for ultrashort pulse generation," *Sci. Rep.*, vol. 6, 2016, Art. no. 20644.
[47] N. H. Park, H. Jeong, S. Y. Choi, M. H. Kim, F. Rotermund, and D.-I. Yeom, "Monolayer graphene saturable absorbers with strongly enhanced evanescent-field interaction for ultrafast fiber laser mode-locking," *Opt. Exp.*, vol. 23, no. 15, pp. 19806–19812, 2015.
[48] Q. Bao *et al.*, "Monolayer graphene as a saturable absorber in a mode-locked laser," *Nano Res.*, vol. 4, no. 3, pp. 297–307, 2011.
[49] M. B. Hisyam, M. F. M. Rusdi, A. A. Latiff, and S. W. Harun, "Generation of mode-locked Ytterbium doped fiber ring laser using few-layer black phosphorus as a saturable absorber," *IEEE J. Sel. Top. Quantum Electron.*, vol. 23, no. 1, pp. 39–43, Jan./Feb. 2017.
[50] T. Chen, Q. Zhang, Y. Zhang, X. Li, H. Zhang, and W. Xia, "All-fiber passively mode-locked laser using nonlinear multimode interference of step-index multimode fiber," *Photon. Res.*, vol. 6, no. 11, pp. 1033–1039, 2018.
[51] X. Han-Ding *et al.*, "Passive harmonic mode-locking of Er-doped fiber laser using CVD-grown few-layer MoS_2 as a saturable absorber," *Chinese Phys. B*, vol. 24, no. 8, 2015, Art. no. 84206.
[52] Y. Yang, S. Yang, C. Li, and X. Lin, "Passively Q-switched and mode-locked Tm-Ho co-doped fiber laser using a WS_2 saturable absorber fabricated by chemical vapor deposition," *Opt. Laser Technol.*, vol. 111, pp. 571–574, 2019.
[53] M. Jung, J. Lee, J. Park, J. Koo, Y. M. Jhon, and J. H. Lee, "Mode-locked, 1.94-μm, all-fiberized laser using WS_2-based evanescent field interaction," *Opt. Exp.*, vol. 23, pp. 19996–20006, 2015.
[54] H. Ahmad, M. Z. Samion, A. A. Kamely, and M. F. Ismail, "Mode-locked thulium doped fiber laser with zinc oxide saturable absorber for 2 μm operation," *Infrared Phys. Technol.*, vol. 97, pp. 142–148, 2019.
[55] J. Sotor, G. Sobon, M. Kowalczyk, W. Macherzynski, P. Paletko, and K. M. Abramski, "Ultrafast thulium-doped fiber laser mode locked with black phosphorus," *Opt. Lett.*, vol. 40, no. 16, pp. 3885–3888, 2015.
[56] S. Yang *et al.*, "Wavelength-adjustable mode-locked Tm-Ho co-doped fiber laser from 1839 nm to 1876 nm," *Opt. Fiber Technol.*, vol. 46, pp. 157–161, 2018.
[57] H. Yu, X. Zheng, K. Yin, T. Jiang, and others, "All-fiber thulium/holmium-doped mode-locked laser by tungsten disulfide saturable absorber," *Laser Phys.*, vol. 27, no. 1, 2016, Art. no. 15102.